RESEARCH ARTICLE

Enhancement in the selectivity of O_2/N_2 via ZIF-8/CA mixed-matrix membranes and the development of a thermodynamic model to predict the permeability of gases

Shakir Ul Azam[1] · Arshad Hussain[1] · Sarah Farrukh[1] · Tayyaba Noor[1] · Yangxian Liu[2]

Abstract
Zeolitic imidazolate framework-8 (ZIF-8) has a sodalite topology. ZIF-8 is composed of zinc ion coordinated by four imidazolate rings. The pore aperture of ZIF-8 is 3.4 Å, which readily retains large gas molecules like N_2. In this work, mixed-matrix membranes (MMMs) have been fabricated by utilizing ZIF-8 and pristine cellulose acetate (CA) for O_2/N_2 separation. Membranes of pristine CA and MMMs of ZIF-8/CA at various ZIF-8 concentrations were prepared in tetrahydrofuran (THF). Permeation results of the fabricated membranes revealed increasing selectivity for O_2/N_2 with increasing pressure as well as ZIF-8/CA concentration up to 5% (w/w). The selectivity of O_2/N_2 increased 4 times for MMMs containing 5% (w/w) of ZIF-8/CA as compared with the pristine CA membrane. A thermodynamic model has also been developed to predict the permeability of gases through polymeric membranes. The results were compared with literature data as well as the pristine CA membrane produced in this work for model validation.

Keywords Gas separation · Mixed-matrix membranes · Cellulose acetate · Membrane fabrication · Metal-organic frameworks · Zeolitic Imidazolate frameworks

Introduction

Gas separation by using membranes has gained momentous importance, owing to its low capital and operating cost, compact size, low energy requirement, no involvement of complex chemicals, environmental friendliness, and ease of operation (Chung et al. 2007). Membrane technology is now replacing other conventional gas separation methods like cryogenic distillation and pressure swing adsorption (Aaron and Tsouris 2005; Mersmann et al. 2000). The current applications of membrane technology include separation of hydrogen, sepa-ration of carbon dioxide, air separation into enriched oxygen and nitrogen, purification of natural gas, and nitrogen recov-ery (Farrukh et al. 2014a, b; Koros and Fleming 1993). For these applications, membranes must have high permeability, selectivity, durability, and mechanical strength (Koros 2002; Koros and Mahajan 2000). The achievement of high selectiv-ity and permeability simultaneously remains a challenge in gas separation (Koros et al. 1988; Pandey and Chauhan 2001; Stern 1994). Polymeric membranes have touched the boundary of the tradeoff of the permeability-selectivity plot described by Robeson (1991). To boost up the performance of membranes, novel materials and procedures have been scruti-nized. Inorganic membranes have been used for gas separation due to their high permeabilities and selectivities (Ismail and David 2001; Weitkamp et al. 2007). Inorganic membranes, however, have low reproducible properties (van de Graaf et al. 1998), low mechanical resistance, and high cost (Caro et al. 2000; Ismail and David 2001), which make their pro-duction difficult. Intensive research work has been done to introduce new hybrid membranes, which encompass the de-sirable properties of organic and inorganic membranes. To achieve this objective, mixed-matrix membranes (MMMs)

Responsible editor: Tito Roberto Cadaval Jr

✉ Sarah Farrukh
Sarah.farrukh@scme.nust.edu.pk

[1] School of Chemical & Materials Engineering (SCME), National University of Sciences & Technology (NUST), Islamabad, Pakistan

[2] School of Energy and Power Engineering, Jiangsu University, Zhenjiang, China

have been introduced (Koros and Mahajan 2000). MMMs combine the higher permeabilities and selectivities of inorganic membranes with the easy processability of polymeric membranes. MMMs have more reproducible properties, are facile and mechanically more resilient, and also have low fabrication costs than inorganic membranes (Caro et al. 2000; Sheffel and Tsapatsis 2007; Iqbal et al. 2019).

Polymers used for continuous phase in MMMs for gas separation in commercial scale are polysulfones, cellulose acetate, polycarbonates, polyarylates, poly(aryl ethers), poly(aryl ketone), polyamides, and polyimides (Baker and Low 2014; Himma et al. 2018; Murali et al. 2013; Sanders et al. 2013). In this study, cellulose acetate (CA) has been chosen as a polymer matrix for the fabrication of MMMs due to its availability, low cost, good performance for O_2/N_2 separation, environmental inertness, and abundant presence of hydroxyl group which can be easily activated by different strategies for the ligand coupling (Haraya et al. 1986a, b; Minhas et al. 2015). The structure of CA is shown in Fig. 1.

Various kinds of materials have been used as an additive in MMMs, comprising zeolites (Moore and Koros 2007; Moore et al. 2003; Sen et al. 2006), carbon molecular sieves (CMS) (Vu et al. 2003a, b), carbon nanotubes (CNTs) (Kim et al. 2007), activated carbons (Esteves and Mota 2007), mesoporous materials (Kim et al. 2006), and metal-organic frameworks (MOFs) (Car et al. 2006; Zhang et al. 2008a). MMMs have crossed the upper bound in Robeson cure for gas separation (Chung et al. 2007), but there are still challenges to overcome. The compatibility of the additive with the polymer matrix is one of the significant challenges. The low affinity among the inorganic additive and the polymer leads to the development of non-selective void at the additive-polymer interface, which reduces the performance of MMMs (Mahajan et al. 2002; Moore et al. 2004; Shu et al. 2007). This low affinity is due to the poor wetting or interfacial contact. Various types of zeolites have been used as an additive in MMMs due to their exceptional gas separation properties and thermal stabilities. Zeolites which have been employed for the fabrication of MMMs are zeolite 4A (Huang et al. 2006b; Li et al. 2005; Mahajan et al. 2002; Moore and Koros 2007; Moore et al. 2003) and zeolite SSZ-13 (Hillock et al. 2008). Zeolites show low compatibility with the matrix of the polymer, and in some cases, they behaved like fillers (Chung et al. 2007; Li et al. 2007; Moore and Koros 2007; Vu et al. 2003a). Different compatibilizers like diblock copolymer (dBC), 2,4,6-triaminopyrimidine (TAP), and 3-(trimethoxysilyl) propylmethacrylate (TMOPMA) have been used to escalate the compatibility between zeolites and polymers in MMMs (Hu et al. 2006; Huang et al. 2006b; Li et al. 2006; Moore and Koros 2008; Patel et al. 2011; Yong et al. 2001); however, significant improvement has not been achieved.

Mesoporous materials have been used as an additive in MMMs to boost up the interaction of polymer and additive, through the penetration of the mesopores by the polymeric chains. This notion was confirmed by using MMMs of MCM-41/polysulfone for gas separation including O_2 (Reid et al. 2001). The permeabilities of various gases increased by increasing the concentration of MCM-41; however, the selectivities remained constant. One of the drawbacks of using mesoporous material as an additive in MMMs is the loss in selectivity due to the mesopores (Zhang et al. 2008b).

Metal-organic frameworks (MOFs) are an advanced type of porous material that has been employed as an additive in MMMs for gas separation including O_2/N_2 separation. These materials consist of metal ions or clusters coordinated to organic ligands to form one-, two-, or three-dimensional structures. The organic ligand functional groups and the metal ions in MOFs may provide a facilitated interaction with the polymer chains. MOFs are famous for having tunable porosity, high surface area, affinity for certain gases, functionalizeable pore walls, diverse pore size and shape, and amendable organic linking units (Ma et al. 2008; Rehman et al. 2019). The incredible properties of MOFs make them an attractive candidate for gas separations, gas storage, and for their use as a

Fig. 1 Cellulose acetate structure

Cellulose acetate
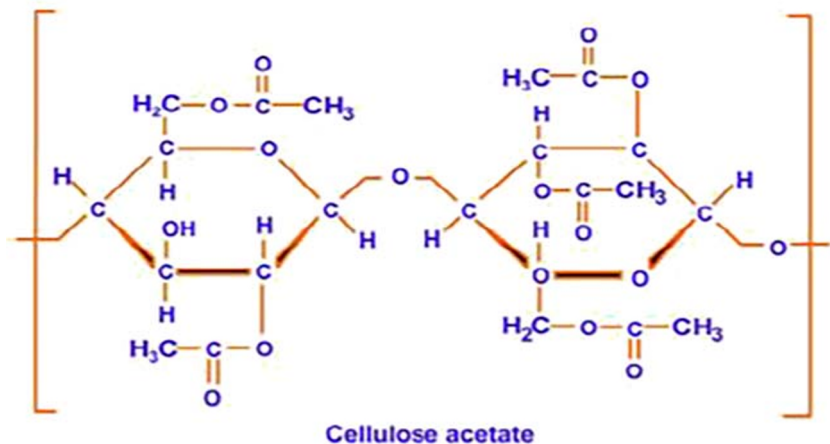
catalyst (Mueller et al. 2006). MOFs have been used extensively for O_2/N_2 separation. MMMs of Matrimid® loaded by MOF-5 as an additive have been studied by Perez et al. (2009) who found that an increased fraction of MOF-5 increases the permeabilities of gases including O_2 and N_2, without substantially changing their selectivities. Zhang et al. (2008a) studied MMMs of Matrimid® loaded by Cu-BPY-HFS, a type of MOF, for gas separations. The resulted MMMs have an enhanced permeability for O_2 from 1.46 to 3.06 barrer deprived of substantial enhancement in the selectivity of O_2/N_2. ZIF-8 a subclass of MOF, which has been used as an additive in Matrimid® to produce ZIF-8/ Matrimid® MMMs for O_2/N_2 separation by Josephine C. et al. (Ordonez et al. 2010). They found that adding ZIF-8 into the matrix of Matrimid® up to 40% (w/w) improved the permeability of O_2 without substantially changing the selectivity.

ZIFs have an excellent chemical and thermal stability (up to 400 °C), tunable porosity, and chemical functionality (Park et al. 2006). ZIFs have structure similar to many zeolite due to its basis on the metal imidazolate (Hayashi et al. 2007). ZIF-8, for example, has sodalite (SOD) topology (Huang et al. 2006a). In ZIF-8 as shown in Fig. 2, the ring of five-membered imidazolate works as a bridge between Zn (II) in the center and divulges angle of $145°$ all around the frameworks by coordinating N-atoms on 1, 3-positions of the ring (Park et al. 2006). $145°$ bond angle formed by metal-imidazolate-metal in ZIFs is analogous to the bond angle made by Si–O–Si in numerous zeolites (Park et al. 2006). Pore aperture of ZIF-8 is 3.4 Å, which is nearly identical to the kinetic diameter of oxygen, which is 3.46 Å and less than that of nitrogen, and which is 3.64 Å (Ghosal and Freeman 1994). The diameter of the pore cavity of ZIF-8 is 11.1 Å and has an extraordinary surface area of 1300–1600 m^2/g (Park et al. 2006). Owing to its attractive properties, ZIF-8 has been selected

in this work as an additive for the fabrication of MMMs. The surface properties of CA define the threshold amount of ZIF-8 required to eradicate the interfacial void. ZIF-8 is expected to form hydrogen bonding with cellulose acetate. The hydrogen bonding formed due to the lone pair electrons in the oxygen contributes to partial negative charge on the oxygen present in cellulose acetate with a partial positive charge on hydrogen atoms present in ZIF-8. The interaction among CA and ZIF-8 is shown in Fig. 3.

In this work, MMMs were fabricated by employing CA as a polymer matrix and ZIF-8 as an additive for the separation of O2/N2. The permeation of pure O2 and N2 was investigated through pristine CA and ZIF-8/CA MMMs. A thermodynamic model was also developed in this work, to predict the permeabilities of gases through polymeric membranes. Permeability prediction is a promising task, and very few researchers have tried to predict the permeability of gases through the membranes. In this work, the model of Lee et al. (2007) is modified by using various correlations to predict the permeability completely. The developed model was then applied to literature data as well as to this work, to predict the permeabilities of gases through pristine CA membrane for verification.

Experimentation

Materials

Cellulose acetate (CA) having $M_n = 50,000$ g/mol and anhydrous tetrahydrofuran (THF) with $\geq 99.9\%$ was obtained from Sigma-Aldrich, St. Louis, MO, USA. ZIF-8 was obtained from our research group. For permeation, commercial grade of O_2 and N_2 gases were used.
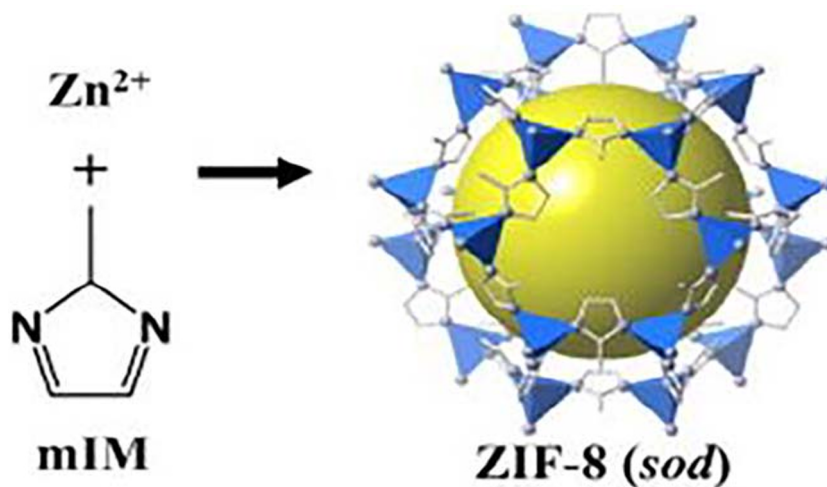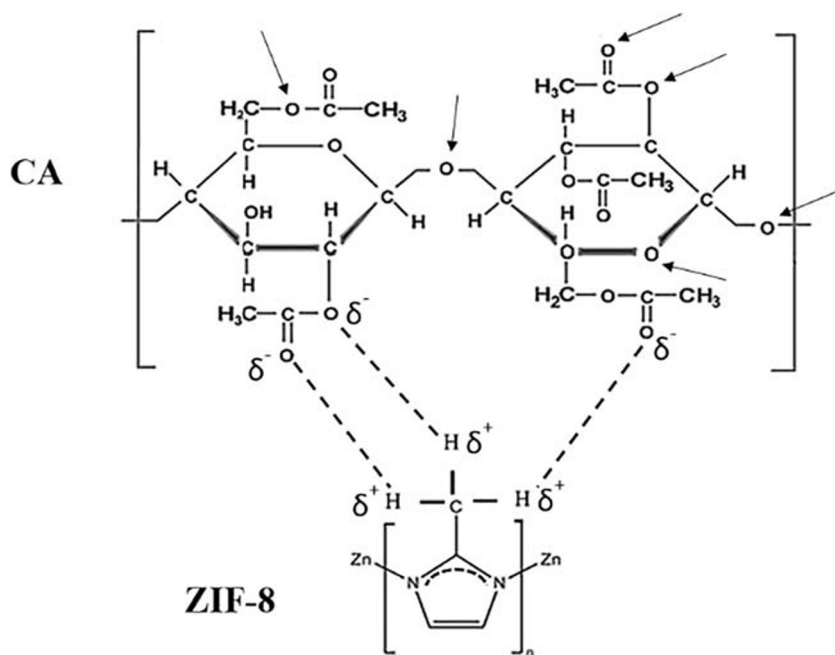
Fig. 2 Structure of ZIF-8

Fig. 3 Interaction among CA and ZIF-8

Fabrication of ZIF-8/CA mixed-matrix membranes

Solution blending technique (Cong et al. 2007) was utilized to fabricate MMMs of ZIF-8/CA (0%, 2%, 3.5%, 5%, 8%, and 11% (w/w)). For pure CA membrane fabrication, 1 g of CA was added to 10 ml THF to make a 10% (w/v) polymer solution. The polymer solution was then stirred by using a magnetic stirrer for 24 h to complete the dissolution of CA into THF. The bubble-free solution was then cast into Petri dishes and dried under atmospheric conditions. For the fabrication of MMMs of 2% (w/w) ZIF-8/CA, 1 g CA was added to 8 ml THF to make an 8% (w/v) polymer solution, and ZIF-8 solution was made by adding 0.02 g of ZIF-8 into 2 ml THF. The stirring of these solutions was done by using magnetic stirrers for 24 h, after which both the solutions were mixed to form the MMM solution. The solution was stirred again for 6 h and then probe sonicated for 2 h to complete dispersion of ZIF-8 nanocrystals into the solution. The solution was further stirred for 2 h, and the bubble-free solution was then cast into Petri dishes. The casted membranes were then dried under atmospheric conditions for 16 h. All the other MMMs of various ZIF-8/CA concentrations, i.e., 3.5%, 5%, 8%, and 11% (w/w), were prepared by utilizing the aforementioned technique of MMMs fabrication.

Characterization and measurement

Fourier transform-infrared spectroscopy (FT-IR) analysis

The various functional groups present in pristine CA, ZIF-8, and ZIF-8/CA MMMs (2%, 3.5%, 5%, 8%, and 11% (w/w)) were analyzed by using FT-IR. The FT-IR analysis was executed by using the Perkin-Elmer spectrum 100 FT-IR Spectrometer. The range used during the analysis was 400–4000 cm^{-1} wavenumber with 4 cm^{-1} resolution.

X-ray diffraction analysis

Crystallinity of pure CA, ZIF-8, and ZIF-8/CA MMMs (2%, 3.5%, 5%, 8%, and 11% (w/w)) were analyzed by using XRD, and the analysis was executed by means of diffractometer of STOE Germany with CU K_{α} Xion-ray radiation. The spectrum of XRD was obtained between 5 and 40° at the rate of 0.04°/s. In the XRD spectrum, peak height, peak width, and peak position express the behavior of particular material.

Scanning electron microscopy (SEM) analysis

SEM analysis of pristine CA, ZIF-8, and MMMs of ZIF-8/CA (2%, 3.5%, 5%, 8%, and 11% (w/w)) were executed by means of JEOL JSM-6490LA analytical low vacuum SEM to analyze the morphology of membranes. The accelerating voltage of 5 kV and 10 kV was used for the analysis at different magnifications.

Tensile strength analysis

Tensile strength of pristine CA and MMMs of ZIF-8/ CA (2%, 3.5%, 5%, 8%, and 11% (w/w)) were tested by means of SHIMADZU AGS-X series precision ultimate tensile tester. The maximum load was 20 kN. The membranes were tested by following the standards of ASTM, D882-02 at 0.5 mm/min strain rate.

Permeation testing

Permeation testing of oxygen and nitrogen through pristine CA and ZIF-8/CA (2%, 3.5%, 5%, 8%, and 11% (w/w)) MMMs at different pressures were executed by using a stainless steel gas permeation testing system with 8 cm^2 active area. The flowrates of the permeating gases were measured by using bubble flow meter against different pressure while at constant temperature. Permeability of both gases was then found by using Eq. (1).

$$P = J \, \frac{l}{\Delta P} \tag{1}$$

where P is the permeability, J is the permeate gas flux, l is the membrane thickness, and ΔP is the pressure difference.

Selectivity (α) of O$_2$/N$_2$ was found by taking the ratio of the permeabilities of O$_2$ (P_{O2}) to the permeabilities of N$_2$ (P_{N2}):

$$\alpha o_{2/N_2} = \frac{(P_{O2})}{(P_{N2})} \tag{2}$$

Results and discussion

Characterization by FT-IR

FTIR spectrum of CA confirmed the presence of different desirable functional groups as can be observed from Fig. 4a. Cellulose acetate exhibited peaks at 3492, 2945, 2889, 1742, 1431, 1378, 1250, 1050, and 604 cm^{-1} (Mark 2009). Absorption band at 3492 cm^{-1} is endorsed to hydroxyl group (OH). Peaks at 2945 and 2889 cm^{-1} are allocated to asymmetric methyl group (CH$_3$) and symmetric methyl group (CH$_3$) stretching, respectively. The peak at 1742 cm^{-1} represents carbonyl stretching (C=O), while the peaks at 1431 and 1378 cm^{-1} are allocated to asymmetric and symmetric methyl group (CH$_3$) deformation, respectively. Peak at 1250 cm^{-1} is credited to C–C–O stretching in the acetate group. Peak at 1050 cm^{-1} represents the stretching manner of C–O, and the absorption band at 604 cm^{-1} represents the structural factor of cellulose acetate.

Absorption bands of ZIF-8 are 3135, 2929, 1574, 1500–1350, 1350–900, 800–600, and 421 cm^{-1} (Hu et al. 2011). These peaks can be observed from Fig. 4b. The absorption bands at 3135 and 2929 cm^{-1} are credited to the aromatic and aliphatic stretching of C–H in the imidazolate, respectively. Absorption band at 1574 cm^{-1} is consigned to C=N stretching. Peaks in between 1500 and 1350 cm^{-1} are credited to the whole ring stretching. Peaks in between 1350 and 900 cm^{-1} are for the ring in-plane bending, while the absorption region in between 800 and 600 cm^{-1} is consigned to the

ring out-plane bending. The band at 421 cm^{-1} is assigned to mode of stretching Zn–N.

No new peak appeared in the MMMs of ZIF-8/CA (2%, 3.5, 5%, 8%, and 11% (w/w)), as can be observed from Fig. 4c, due to the physical interaction between CA and ZIF-8 through hydrogen bonding, which is an intermolecular force attraction. The peaks that appeared in the FT-IR spectrum of mixed-matrix membranes are endorsed from CA and ZIF-8. The absorption bands that appear in ZIF-8/CA MMMs are 3492, 2945, 2889, 1742, 1574, 1050, 604, and 421 cm^{-1}. The band at 3492 cm^{-1} confirmed the existence of the hydroxyl group (OH) of the polymer phase (CA) in all the MMMs. The presence of peaks at 2945 and 2889 cm^{-1} confirmed the existence of asymmetric and symmetric methyl group (CH$_3$) in the polymer phase (CA) of all the MMMs. Peak at 1742 cm^{-1} confirmed the existence of the carbonyl group (C=O) in the polymer phase (CA) of all the MMMs. Absorption band at 1574 cm^{-1} confirmed the occurrence of C=N of ZIF-8 in all the MMMs. Absorption band at 1050 cm^{-1} confirmed the existence of C–O in all the MMMs, which is present in CA. The sharp band at 604 cm^{-1} represented the structural factor of the continuous phase (CA) in all the MMMs. Absorption band at 421 cm^{-1} ensured the existence of Zn–N stretching in the MMMs, which is present in ZIF-8.

Characterization by XRD

The patterns of XRD were acquired between 5 and 40° at the rate of 0.04°/s. In the XRD spectrum, the peak height, width, and position express the structural behavior of particular material. XRD results of CA, ZIF-8, and MMMs of ZIF-8/CA (2%, 3.5%, 5%, 8%, and 11% (w/w)) are shown in Fig. 5.

The orderly arrangement of polymer chains originates crystallinity, while loose packing of polymer chains results in amorphous nature. Polymers have some crystalline parts, while other parts are amorphous. Thus, in the spectrum of XRD, sharp and high-intensity peaks indicate the crystalline phase, whereas wide and low-intensity peaks indicate an amorphous phase. The XRD spectrum of pristine CA shows a diffuse wide peak at 2θ = 18.2° with maximum intensity. CA is a semi-crystalline polymer, and its crystallinity is reduced by hydrogen bonding between acetyl and hydroxyl group.

XRD spectrum of ZIF-8 shows robust peaks at 2θ = 7.20, 10.28, 12.56, 14.58, 16.32, 17.92, 22.6, 24.36, 25.44, 26.48, and 29.52°, corresponding to planes (011), (002), (112), (022), (013), (222), (114), (223), (224), (134), and (044). These peaks were well satisfied by literature (Zhou et al. 2017). The sharp and strong peaks of ZIF-8 can be seen in all the MMMs of ZIF-8/CA (2%, 3.5%, 5%, 8%, and 11% (w/w)). The crystallinity increases from pure CA to MMM of ZIF-8/CA 11% (w/w).
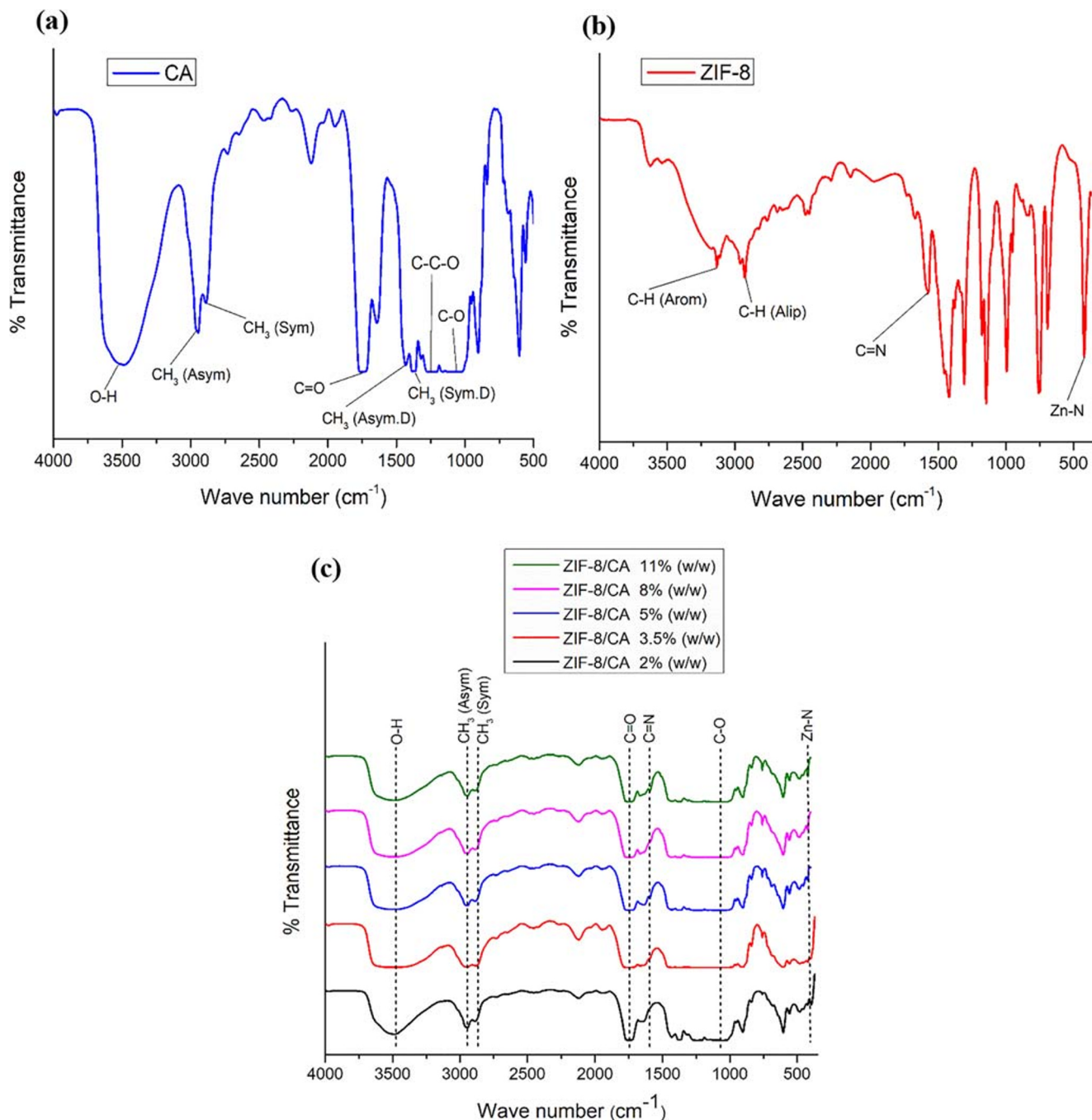
Fig. 4 FT-IR spectrum of **a** CA, **b** ZIF-8, and **c** ZIF-8/CA (2%, 3.5, 5%, 8%, and 11% (w/w)) MMMs

Characterization by SEM

SEM images were acquired for the surface as well as cross-section with different concentrations of ZIF-8/CA, as presented in Fig. 6. All the samples were analyzed at various magnifications. The surface SEM image of pristine CA shows that it is completely smooth and dense. Its cross-section image also confirmed that there is no void in the matrix. The interaction of ZIF-8 with polymer matrix is high, because of its large

surface area and hybrid nature. At a lower concentration of ZIF-8/CA, i.e., 2% (w/w), very few particles can be observed on the surface of the membrane, and the cross-section is also void free. As the concentration of ZIF-8/CA is increased from 2 (w/w) to 3.5% (w/w), more particles can be observed on the top of the surface, but the dispersion of additive particles is not uniform at this concentration.

Defect-free and homogenous dispersion of ZIF-8 can be observed at a 5% (w/w) concentration of ZIF-8/CA. The
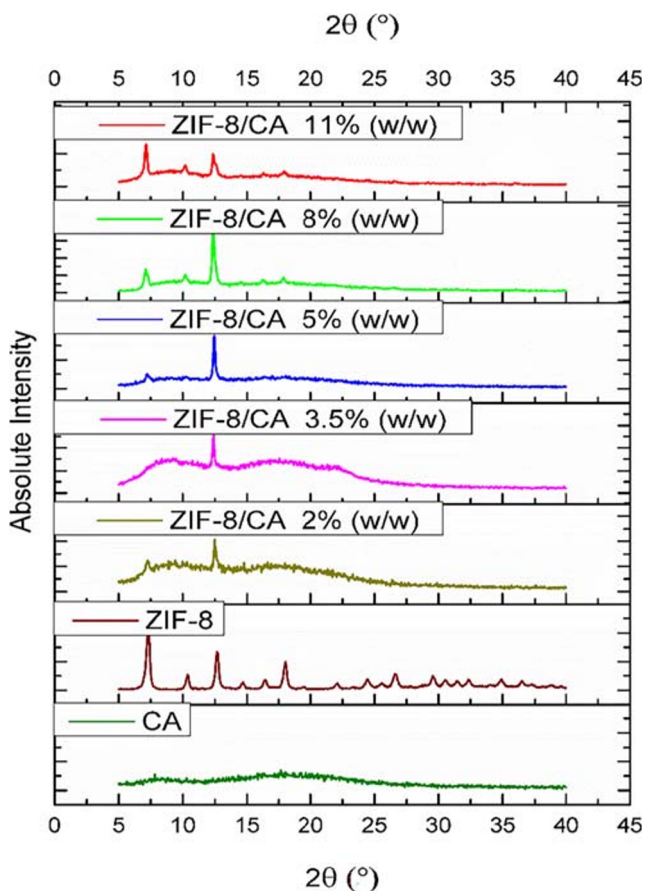
Fig. 5 XRD plots of CA, ZIF-8, and ZIF-8/CA (2%, 3.5%, 5%, 8%, and 11% (w/w)) MMMs

uniformity of ZIF-8 particles can also be observed from the cross-section of this membrane. At ZIF-8/CA concentration above 5% (w/w), i.e., 8% (w/w), the particles became aggregated, which lead to the formation of cavities (Kim et al. 1996; Zhang et al. 2003) as observed from both the surface and the cross-section. The agglomeration of ZIF-8 nanocrystals is more predominant at ZIF-8/CA concentration of 11% (w/w), which diminished the membrane performance.

Characterization by tensile testing

The results of the tensile strength analysis of all the fabricated membranes are shown in Fig. 7. Tensile tests were executed for a number of samples to find out the standard deviation. Tensile strength of pure CA is greater than ZIF-8/CA MMMs (2%, 3.5%, 5%, 8%, and 11% (w/w)). Pure CA is completely smooth and dense as depicted from SEM images; therefore, its strength is also high. As the concentration of ZIF-8/CA was increased, the resultant membranes indicated lesser strength, which is due to the physical interaction of CA and ZIF-8. The interaction of CA and ZIF-8 was high at a lower concentration of ZIF-8/CA MMMs but still lower than pristine CA, and as

the concentration was increased, agglomeration of ZIF-8 particles formed into the CA matrix, which reduced the tensile strength of the resultant MMMs. The agglomeration of ZIF-8 nanocrystals into the CA matrix can also be ratified from SEM images. Analogous trends of results were also acquired by Josephine C. et al. (Ordonez et al. 2010) for their MMMs of ZIF-8/Matrimid.

Permeability testing

Permeability testing was carried out at different pressures for pure O_2 and N_2 through pristine CA and MMMs of ZIF-8/CA at different concentrations, i.e., 2%, 3.5%, 5%, 8%, and 11% (w/w). Reproducibility of MMMs is very important due to the inadequate distribution of additive particles into the matrix of polymer; therefore, the membranes were casted multiple times to achieve a methodology that reproduces the results.

All the membranes were fabricated at least three times and tested for permeation for both gases (O_2 and N_2), and standard deviation for all the membranes was found at different pressures, which reflects the error of permeation testing. Two parameters, i.e., pressure and concentration of ZIF-8/CA (% w/w), affect the permeation of O_2 and N_2 through the fabricated membranes.

Effect of pressure on permeation of O_2 and N_2

The permeabilities of both pure O_2 and N_2 and the selectivities of O_2/N_2 at varying pressure through the fabricated membranes are shown in Fig. 8. ZIF-8 has structure similar to zeolites; therefore, it has sieving property (Ordonez et al. 2010). ZIF-8 has 3.40 Å pore aperture, which is nearly equal to the kinetic diameter of O_2 (3.46 Å) and less than N_2 (3.64 Å) (Ghosal and Freeman 1994). For pristine CA, by increasing the pressure difference, the free volume of the polymer decreases due to the hydrostatic compression, and the molecular sieving phenomenon enhanced (Isfahani et al. 2016a, b); therefore, the permeability of O_2 improved slightly, and the permeability of N_2 decreased significantly.

For the MMMs having a concentration of 2%, 3.5%, and 5% (w/w) of ZIF-8/CA, as the pressure difference was increased, the permeabilities of both O_2 and N_2 decreased, and the selectivities of O_2/N_2 increased, which was because the permeability is inversely related to the pressure difference and also due to the compression of polymeric chains which affect the free volumes of polymeric chains. The transport properties are therefore controlled by ZIF-8, which has an excellent sieving property for small gas molecules like O_2. The selectivity of O_2/N_2 is highest for the MMMs having a concentration of 5% (w/w) of ZIF-8/CA and at 4 bar pressure difference. This is the threshold loading of ZIF-8 into the matrix of CA, and the particles of ZIF-8 are completely and homogenously dispersed throughout into the matrix of CA; therefore, the
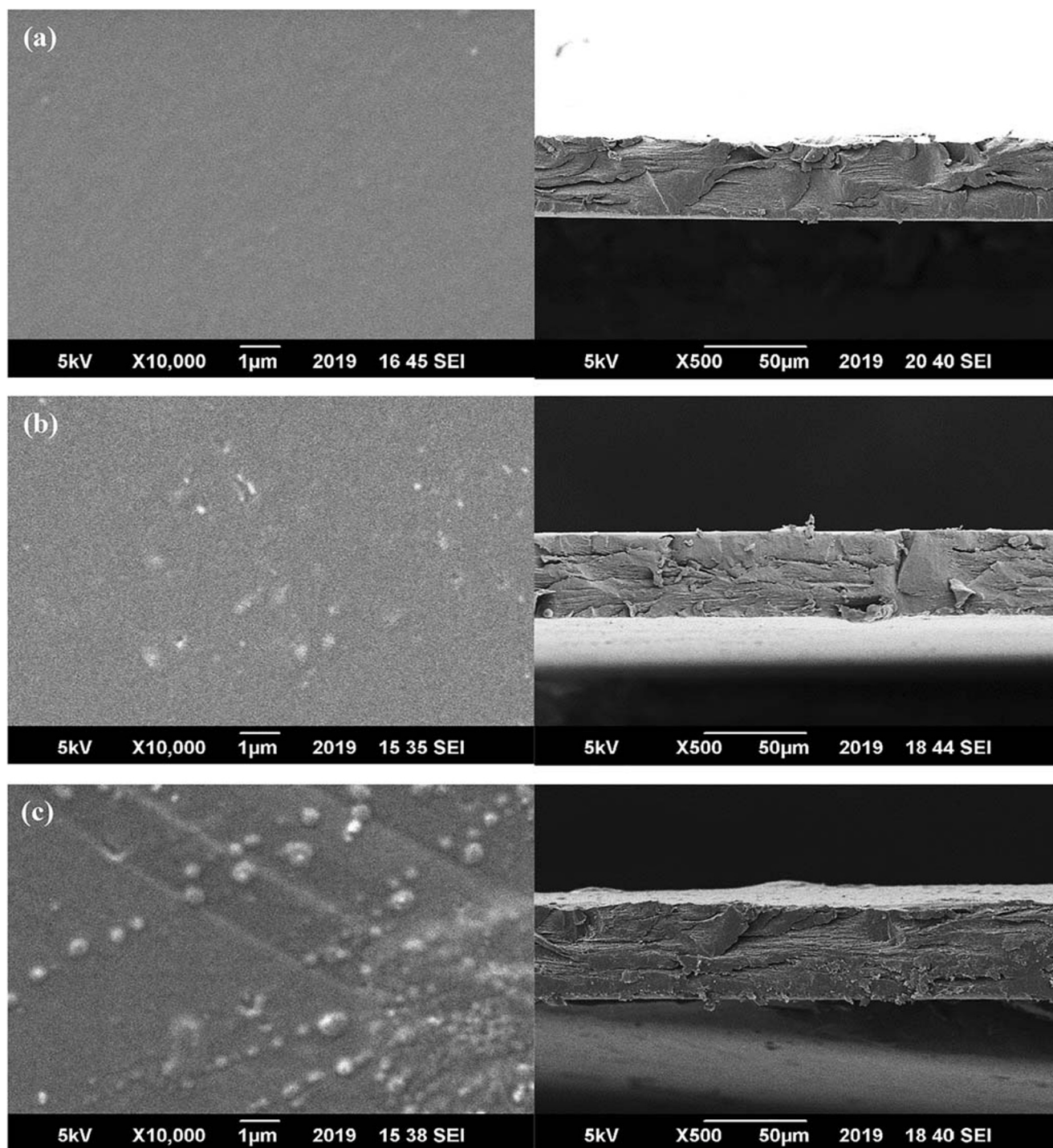
Fig. 6 SEM images of surfaces (left) and cross-sectional (right) of **a** pristine CA and MMMs of ZIF-8/CA **b** 2%, **c** 3.5%, **d** 5%, **e** 8%, and **f** 11% (w/w)

permeation is controlled by ZIF-8 which has an excellent sieving property for small gas molecules and at high pressure, i.e., at 4 bar; the polymer chains become compressed, and the free volume is affected. Molecular sieving occurs for small gas molecules like O_2; therefore, the selectivity of O_2/N_2 increases from pristine CA to 5% (w/w) of ZIF-8/CA MMMs by increasing the pressure as depicted from Fig. 8c. Above this

concentration ,i.e., 8% and 11% (w/w) of ZIF-8/CA, for all the pressure differences, the selectivity of O_2/N_2 decreased abruptly, due to lesser availability of polymer chains to interact with the particles of ZIF-8 causing the formation of agglomerates of ZIF-8 particles into the matrix of CA, which lead to the formation of non-selective void, ultimately decreasing the selectivity of O_2/N_2.
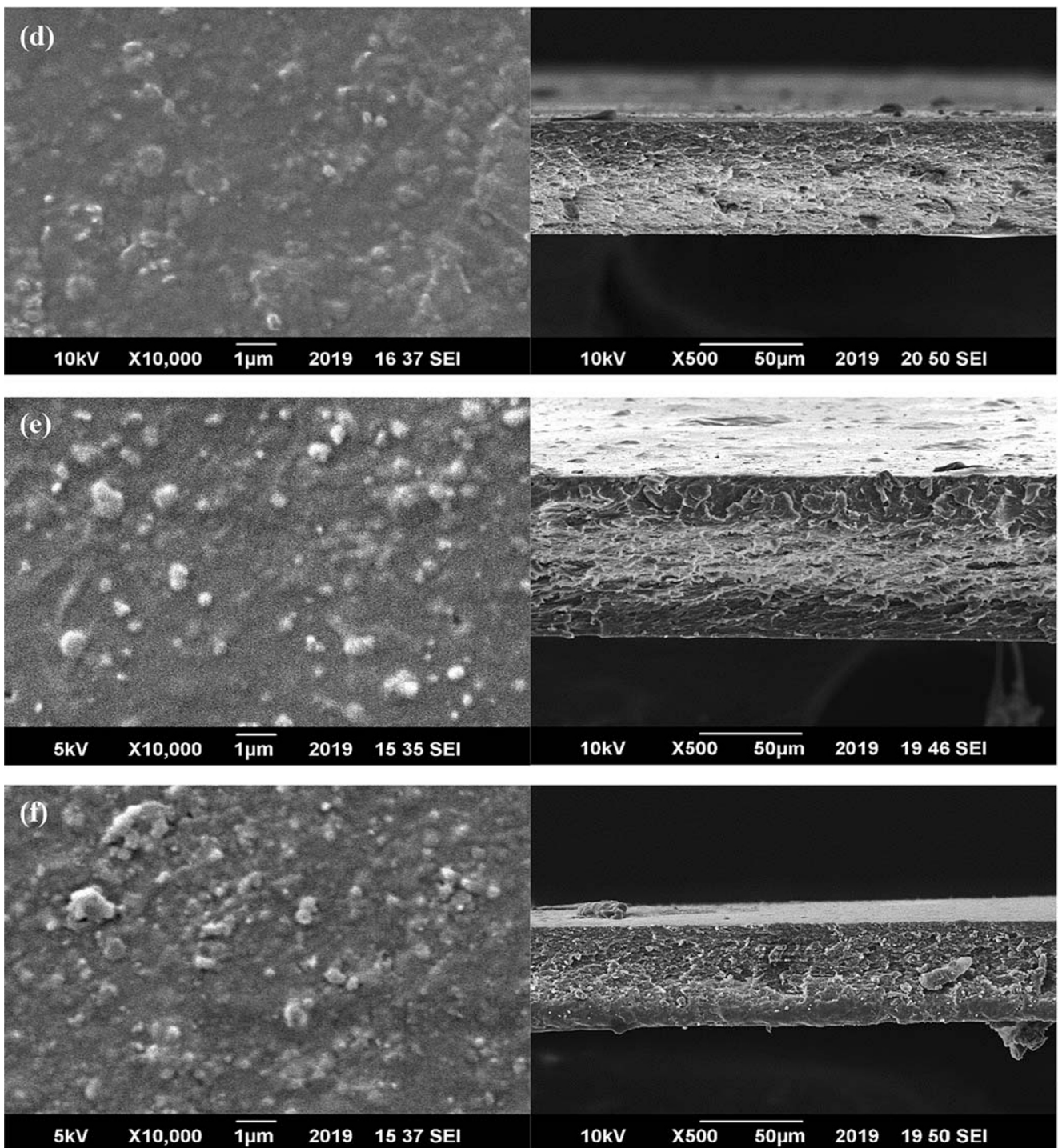
Fig. 6 (continued)

Effect of additive concentration on permeation of gases

In the pristine CA membrane, permeation is controlled by the polymer matrix. When an amount of ZIF-8 is added into the polymer matrix, it becomes rigid, and the permeation is controlled by both the polymer continuous phase and dispersed additive, i.e., ZIF-8 phase. When the concentration of additive is increased up to a certain threshold point, such that the additive is completely and homogeneously dispersed into the polymer matrix, the permeability is controlled by the additive, and the concentration above this point causes the
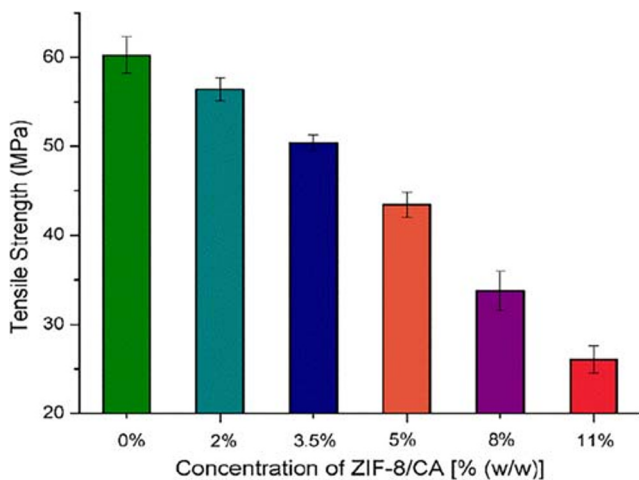
Fig. 7 Ultimate tensile strength of ZIF-8/CA MMMs (0%, 2%, 3.5%, 5%, 8%, and 11% (w/w))

formation of agglomerates of additive particles, which then results in the development of non-selective void. These voids enhance the permeability of both O_2 and N_2 by decreasing the selectivity of O_2/N_2.

The permeability of O_2 in pristine CA and 2% (w/w) ZIF-8/CA MMMs are almost identical, above this concentration, the permeability of O_2 increases, up to the concentration of 8% (w/w) ZIF-8/CA and further increase in the concentration of ZIF-8/CA, i.e., 11% (w/w) causes very little change in the permeability O_2 as depicted from Fig. 9a,. The permeability of N_2 decreases from pristine CA to 5% (w/w) of ZIF-8/CA MMMs and then increases drastically at higher concentrations of ZIF-8/CA. This decrease in the permeability of N_2 as depicted in Fig. 9b reveals the excellent rejection of N_2 and also the threshold loading of ZIF-8/CA, i.e., 5% (w/w). The increase in permeability of N_2 above the concentration of 5% (w/w) of ZIF-8/CA is due to the aggregation of ZIF-8 particles into the matrix of CA, which causes the development of non-selective void (Dong et al. 2013), which results in the increase in the permeabilities of both gases and decrease in the selectivity of O_2/N_2 as depicted from Fig. 9c. The agglomeration of ZIF-8 nanocrystals into the matrix of CA can also be ratified from SEM images. The maximum selectivity of O_2/N_2 has been achieved at 5% (w/w) ZIF-8/CA MMMs.

Development of thermodynamic model to predict the permeability

A model based on configurational entropy was initially developed by Gibbs and DiMarzio (1958) and Gibbs and co-workers (Adam and Gibbs 1965; Dimarzio and Gibbs 1963) for properties of the polymers and used effectively to predict conductivity behavior in polymer electrolytes (Kim and Bae 1999a, b; MacFarlane et al. 1995). Lee et al. (Lee et al. 2007) have developed a thermodynamic model to predict the permeability of gases in polymeric membranes. In this work, the

model developed by Lee et al. (2007) is modified by combining with other correlations to completely predict the permeability of gases through polymeric membranes. Membrane-based gas separation process is considered as an activated process, which can be written in the form of the Arrhenius type equation:

$$P = A \exp\left[-\frac{E_P}{RT}\right] \tag{3}$$

where P is the permeability, E_P is the activation energy, A is the temperature-independent constant, R is the ideal gas constant, and T is the temperature (K).

Permeability can also be expressed as:

$$P = D \cdot S \tag{4}$$

where D is the diffusivity and S is the solubility.

The solubility is a thermodynamic parameter, and diffusivity is a transport parameter, and both can be expressed as Arrhenius type of equation:

$$S = S_o \exp\left[-\frac{\Delta H_s}{RT}\right] \tag{5}$$

$$D = D_o \exp\left[-\frac{E_d}{RT}\right] \tag{6}$$

where S_o is the solubility coefficient, D_o is the diffusivity coefficient, and both are temperature-independent constants. ΔH_s is the heat of solution or sorption, and E_d is the activation energy of diffusion.

Substituting Eqs. (5) and (6) into Eq. (4) gives:

$$P = S_o D_o \ exp\left[-\frac{(\Delta H_s + E_d)}{RT}\right] = P_o exp\left[-\frac{E_d}{RT}\right] \tag{7}$$

$$E_P = \Delta H_s + E_d \tag{8}$$

Assume $T >> T_o$ (the temperature where free volume disappears), Eq. (5) yields:

$$S = S_o \ exp\left[-\frac{\Delta H_s}{R(T-T_o)}\right] \tag{9}$$

Adam and Gibbs (Gibbs and DiMarzio 1958) assume $(T-T_o) = Tln\left(\frac{T}{T_o}\right)$, substituting in Eq. (9) gives:

$$S = S_o \left[-\frac{\Delta H_s}{RTln\left(\frac{T}{T_o}\right)}\right] \tag{10}$$

Total molar configurational entropy S_C^T and temperature are correlated as (Adam and Gibbs 1965; Dimarzio and Gibbs 1963; Gibbs and DiMarzio 1958):
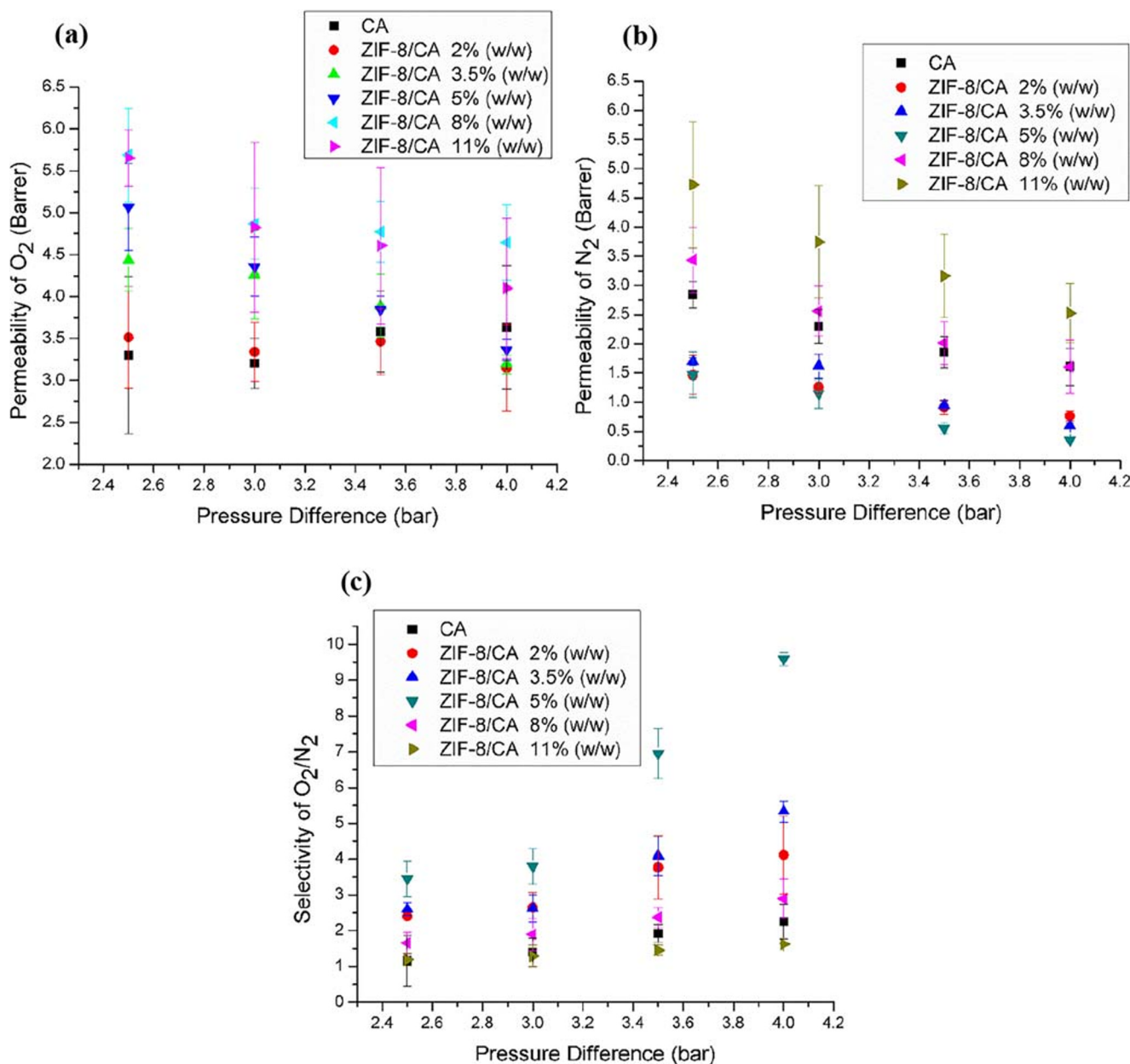
Fig. 8 Effect of pressure difference on permeabilities **a** O_2, **b** N_2, and **c** selectivities of O_2/N_2

$$S_C^T(T)-S_C^T(T_o) = \int_{T_o}^{T} \frac{\Delta C_p}{T}dT = \Delta C_p\ln\left(\frac{T}{T_o}\right) \qquad (11)$$

where ΔC_p is the change in the specific heat of polymer between equilibrium melt (T_m) and glass transition temperature (T_g); therefore, $T_o\left[S_C^T(T_o)\right] = 0$, and Eq. (11) becomes:

$$S_C^T = \int_{T_o}^{T} \frac{\Delta C_p}{T}dT = \Delta C_p ln\left(\frac{T}{T_o}\right) \qquad (12)$$

Substituting Eq. (12) into Eq. (10) yields:

$$S = S_o\left[-\frac{B}{\frac{S_C^T}{k_B}}\right] \qquad (13)$$

$$B = \frac{\Delta H_s \Delta C_p}{RTk_B} \qquad (14)$$

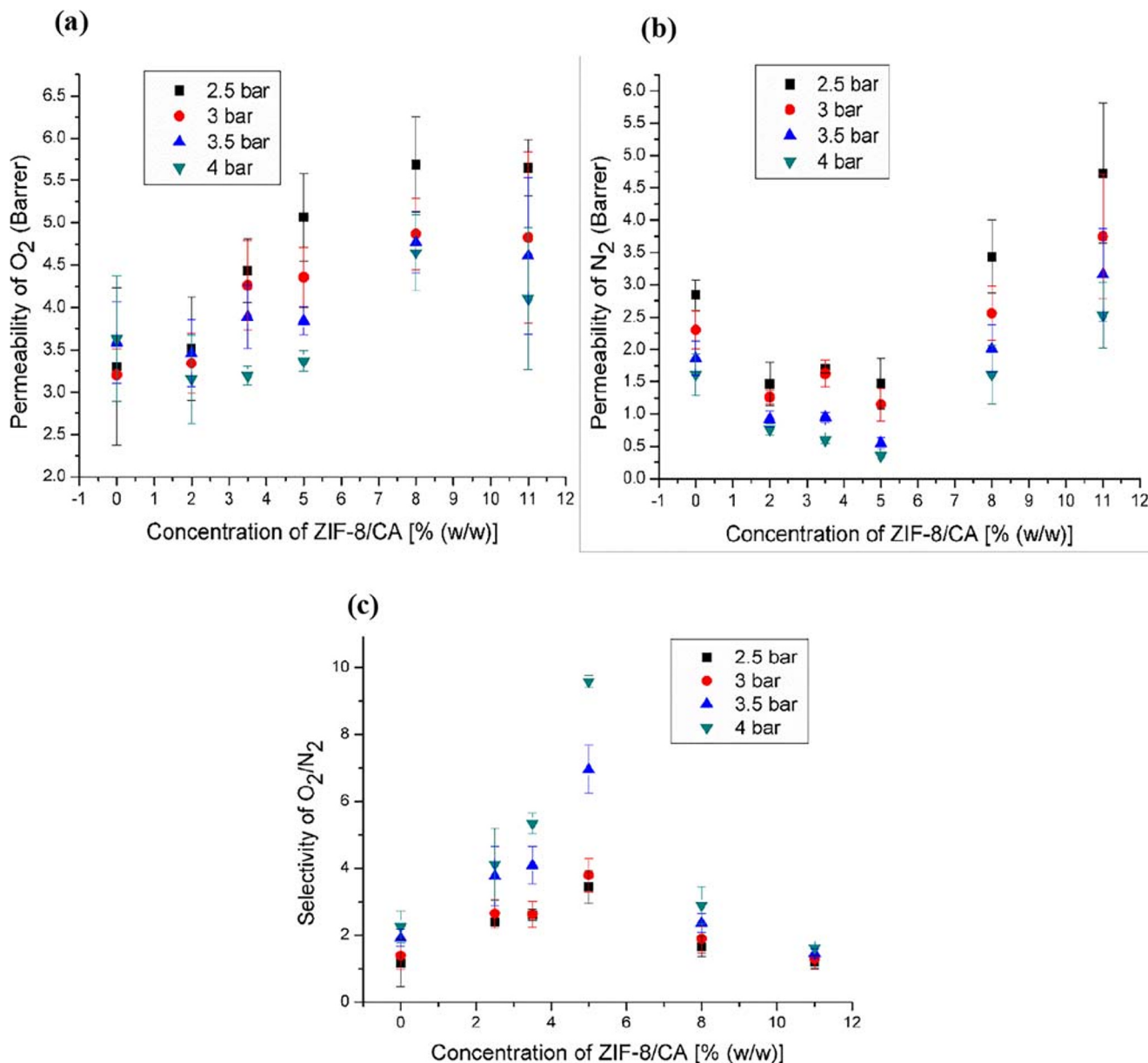where k_B is the Boltzmann constant.

Fig. 9 Effect of concentration of additive (ZIF-8/CA) on permeabilities of **a** O_2, **b** N_2, and **c** selectivities of O_2/N_2

Substituting Eq. (13) into Eq. (4) yields:

$$P = D \cdot S = D \cdot S_o \left[-\frac{B}{\dfrac{S_C^T}{k_B}} \right] \qquad (15)$$

This equation states that for polymeric membranes, the increase in total configuration entropy (S_C^T) in the system of polymer (p)/gas (g) increases the gas permeability.

S_C^T for the system of polymer (p)/gas (g) is the sum of polymer disorientation entropy (S_{dis-p}), polymer and gas mixing entropy (S_{Mix-pg}), and polymer to gas specific interaction entropy (S_{spe-pg}).

$$S_C^T = S_{dis-p} + S_{Mix-pg} + S_{spe-pg} \qquad (16)$$

The polymer disorientation entropy and mixing entropy of polymer-gas increase the total configuration entropy, while specific interaction entropy of polymer to gas reduces the total configuration entropy, as shown in Fig. 10. The entropies are expressed as follows (Flory 1953; Ghosal and Freeman 1994; Kim and Bae 1999a, b; Kim et al. 2000):

$$S_{dis-p} = k_B \frac{\varnothing_P}{r_P} \left[\left(ln\left(r_P \right) + (r_P - 1) ln\left(\frac{z-1}{e} \right) \right) \right] \qquad (17)$$

$$S_{mix-pg} = k_B \left(\frac{\varnothing_P}{r_P} ln\varnothing_P + \frac{\varnothing_g}{r_g} ln\varnothing_g \right) \qquad (18)$$
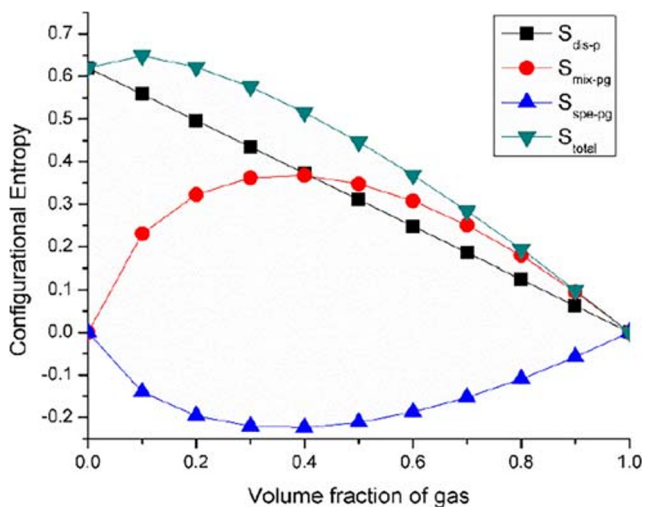
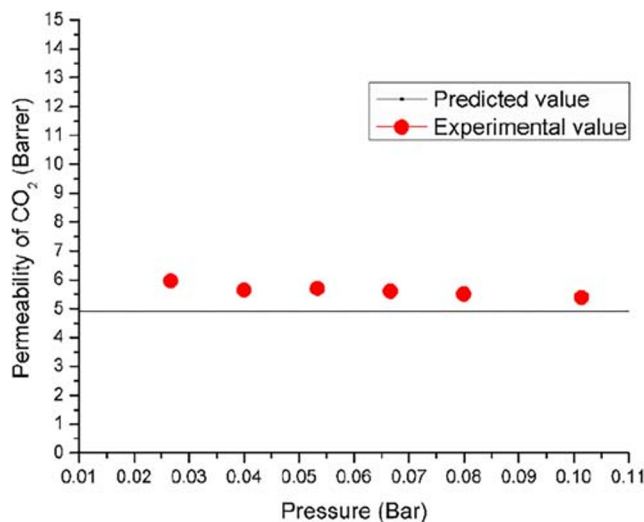**Fig. 10** Change in S_C^T as a function of $\varnothing_g$

Fig. 11 Permeabilities of CO_2 through CA. Solid line was calculated by using Eq. (15), and experimental values were taken from the study of Li et al. (1998)

$$S_{spe-pg} = \gamma_{spe}k_B ln\left(\frac{z-1}{e}\right)\left(\frac{\varnothing_P}{r_P}ln\varnothing_P + \frac{\varnothing_g}{r_g}ln\varnothing_g\right) \quad (19)$$

where $\varnothing_P = r_p n_p/(r_p n_p + r_g n_g)$ and $\varnothing_g = r_g n_g/(r_g n_g + r_p n_p)$ are the volume fraction of polymer and gas, respectively. $r_p = v_p/v_o$, and $r_g = v_g/v_o$, where v_p is the molar volume of polymer, v_g is the molar volumes gas, v_o is the unit lattice volume, and $z = 6$, which is the lattice coordination number. γ_{spe} is the constant of proportionality, demonstrating the specific interaction between polymer and gas. This study will assume $\gamma_{spe} = 1$ for all the cases.

Diffusivity coefficient (D_o) in Eq. (6) can be found by using the following equation reported by Barrer (1942) and Van Amerongen (1946):

$$ln D_{oA} = a\frac{E_{dA}}{RT} - b \quad (20)$$

where a and b are constant and are independent on type of gas. a is also independent on type of polymer, and its value is 0.64, and $b = 11.50$ for glassy polymers and 9.20 for rubbery polymers. These values give the unit in cm^2/s for the diffusion coefficient.

Rearrange Eq. (20), and put into Eq. (6) yields:

$$D = \exp\left(a\frac{E_{dA}}{RT} - b\right)\exp\left(-\frac{E_d}{RT}\right) \quad (21)$$

Solubility coefficient (S_o) can be found by using the Van Krevelen equation (Matteucci et al. 2006), which is:

$$ln S_A = M + N\frac{\varepsilon_A}{k} \quad (22)$$

where M and N are constants. N has a universal value of 0.023 (Van Krevelen and Te Nijenhuis 2009). The value of M differs with the change in the chemical structure of polymer, polymer-penetrant interaction, and free volume of the polymer. Van Krevelen suggests the value of $M = -9.84$ for glassy polymer (Van Krevelen and Te Nijenhuis 2009). The unit of solubility coefficient yields in $cm^3(STP)/(cm^3 cmHg)$ for the values of M and N. ε_A/k is Lennard-Jones temperature of the gas and is listed in Table 1 (Van Krevelen and Te Nijenhuis 2009).

Van Amerongen found that heat of sorption (ΔH_s) is intensely associated with the Lennard-Jones temperature of the gas, after measuring numerous gases solubility in the range of elastomers as a function of temperature (Van Amerongen 1964). Equation (23) also holds well for glassy polymers (Rowe et al. 2010).

Table 1 Penetrant condensability parameters (Van Krevelen and Te Nijenhuis 2009)

Penetrant	ε_A/k (K)
CO_2	195
O_2	71
N_2	107

Table 2 Molecular weights, densities, and molar volumes

Components	M_W (g/mol)	Density (g/cm³)	Molar volume (cm³/mol)	Partial molar volume (V_2) (cm³/mol)
CA	50,000	1.3	38,461.58	–
CO_2	44	0.6 [l]	73.33	45
N_2	28	0.8 [l]	35.00	48
O_2	32	1.141 [l]	28.045	47

[l] Value at liquid state

Table 3 Model equation parameters values

Gas	$D \cdot S_o(10^{-10})$	B	r_g	r_p	E_p (j/mol)	$-\Delta H_S$ (j/mol)	E_d (j/mol)
CO_2	5.04	0.015	1	524.47	8950	23,450	32,400.00
N_2	1.05	0.001	1	1098.90	21,500	1745.94	23,245.94
O_2	3.02	0.003	1	1371.39	16,200	4738.98	20,938.98

$$\frac{\Delta H_s}{R} = 500 - 10\frac{\varepsilon_A}{k} \qquad (23)$$

Equation (15) is the model equation to predict the permeability of gases through polymeric membranes. Volume fraction of permeating gas through polymer can be found by using the following equation (Merkel et al. 2000):

$$\varnothing_g = \left[1 + \frac{22414}{CV_2}\right]^{-1} \qquad (24)$$

where C is the penetrant concentration in polymer, and its unit is (cm^3(STP)/cm^3), and V_2 is the penetrant partial molar volume (cm^3/mol).

$$C = S \cdot P \qquad (25)$$

where S is the solubility and P is the pressure.

Substituting Eq. (25) in Eq. (24) yields:

$$\varnothing_g = \left[1 + \frac{22414}{S \cdot P \cdot V_2}\right]^{-1} \qquad (26)$$

From Eq. (26), experimental values can be compared with predicted values by substituting this equation in the entropy equations in terms of volume faction of gas ($\varnothing_g$), and by setting the volume fraction of polymer ($\varnothing_p$) = 1 - $\varnothing_g$, the obtained plot will be permeability vs pressure.

Results and discussion

The change in the total configurational entropy (S_C^T) of polymer (p)/gas (g) system as a function of volume fraction of gas ($\varnothing_g$) is shown in Fig. 10. The total configurational entropy is found by using Eq. (16). The parameters used to calculate the entropy terms are: M_{wp} = 50,000 g/mol, M_{wg} = 44 g/mol, density of polymer = 1.3 g/cm^3, density of gas 0.8 g/cm^3, and z = 6. By increasing the gas volume fraction ($\varnothing_g$), the polymer disorientation entropy (S_{dis-p}) decreased linearly, probably due to the abridged number of accessible chains of polymer. Entropy of mixing (S_{Mix-pg}) exhibits a maximum value at 0.4 volume fraction of gas ($\varnothing_g$), due to the huge difference between molar volumes of polymer and gas system. The specific interaction entropy (S_{spe-pg}) shows always a negative entropy value, implying that the total entropy of a system is decreased by interaction between two components. Thus, total configurational entropy S_C^T shows a maximum value at 0.1 volume fraction of gas ($\varnothing_g$), and above this value, total configurational entropy (S_C^T) decreased and approaches to zero.

Experimental values have been compared with the model equation for the model validation. Figure 11 represents the permeability of CO_2 through pristine cellulose acetate (CA)
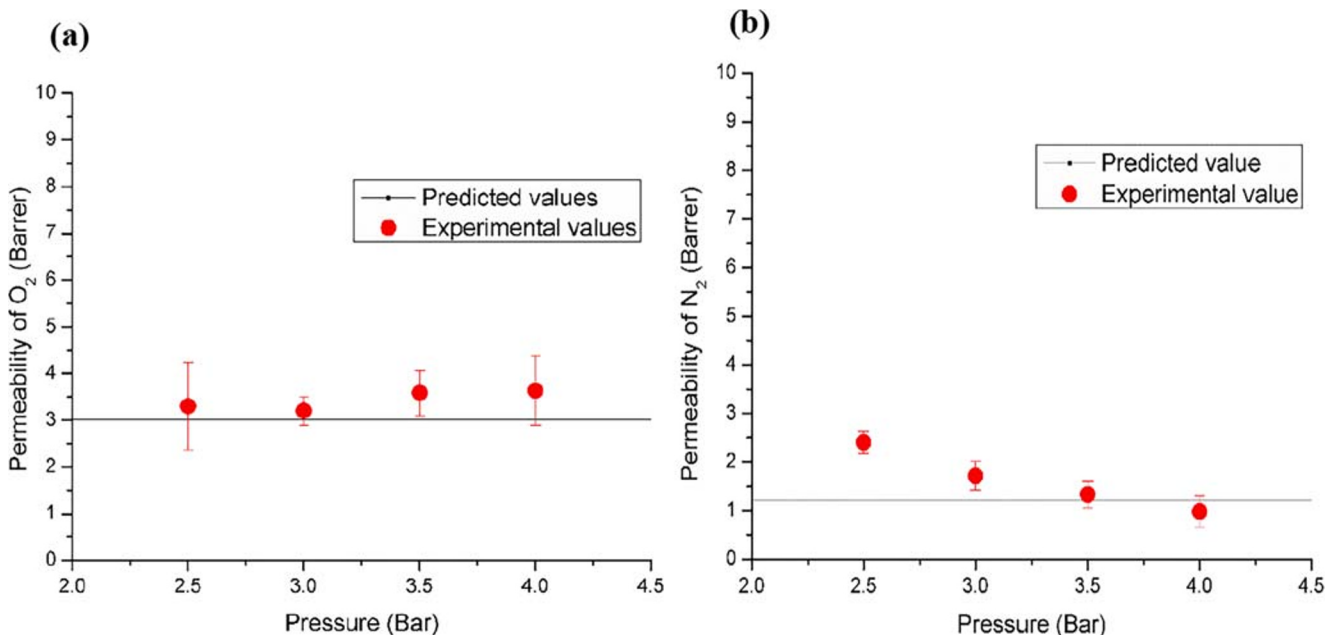

Fig. 12 Permeabilities of **a** O_2 and **b** N_2 through CA. Solid lines were calculated by using Eq. (15), and experimental values were associated with this work

membrane. The solid line represents the predicted permeability by using model Eq. (15), and experimental values have been taken from measured data by Le at al. (Li et al. 1998). The model parameter values for the prediction of CO_2 are shown in Tables 2 and 3. Experimental values are compared with predicted values by using Eq. (26).

Diffusivity of CO_2 through CA has been measured by using Eq. (21), and the sorption coefficient has been measured by using Eq. (22). Although the experimental values are a little bit above the predicted line, he model has successfully predicted the permeability values at the experiment temperature.

Heat of sorption values for O_2 and N_2 has been calculated by using Eq. (23), and activation energies of permeations have been taken from literature (Haraya et al. 1986a). The model parameters to predict the permeabilities of O_2 and N_2 are tabulated in Tables 2 and 3. Figure 12 shows the permeabilities of O_2 and N_2 through the pristine CA membrane. The solid lines were calculated by using the model Eq. (15) for permeability prediction. Experimental data were taken for both O_2 and N_2 from this work. The permeabilities of O_2 and N_2 with standard deviation values somehow follow the predicted permeability line, and the model had predicted the permeabilities successfully.

The deviation in the predicted permeabilities lies in both membrane fabrication conditions and the model equation. The membrane fabrication conditions which affect the morphology of fabricated membranes include the evaporation rate of solvent, the humidity of the surrounding environment, and drying temperature. The variation in the model equation is due to the use of different co-relations; each co-relation has its own percentage error which affects the prediction of permeability.

Conclusion

MMMs were fabricated by using ZIF-8 as an additive and CA as a polymer matrix for O_2/N_2 separation. Both these materials were selected due to their excellent properties and compatibility. Their compatibility has been analyzed, where no chemical change occurs, and both materials hold each other by means of hydrogen bonding, which is an electrostatic force of attraction. ZIF-8 has a pore size approximately equal to the kinetic diameter of O_2; therefore, it has provided sieving property for O_2 and retained N_2. The produced membranes were more selective toward O_2 as compared with N_2 at high pressure and at an additive concentration up to 5% (w/w) of ZIF-8/CA; above this concentration of ZIF-8, membranes lost its selectivity as its permeability increased for both gases. Characterization was done by using FT-IR, SEM, XRD, and tensile testing. FT-IR confirmed that there was only physical interaction present between ZIF-8 and CA. From XRD, it was deduced that by amalgamation of ZIF-8 into the polymer matrix, its crystallinity increases from pristine CA to higher concentration of ZIF-8/CA based MMMs. SEM images confirmed that at higher concentration, agglomeration of ZIF-8 particles formed, which cause the development of non-selective void and which ultimately reduced the performance of the fabricated MMMs. The tensile strength of all the fabricated membranes were measured, which revealed that at higher concentration of ZIF-8 into the polymer matrix, membranes lost their strength due to agglomeration of ZIF-8 nano-crystal into the matrix of CA. Moreover, a thermodynamic model had been developed to completely predict the permeabilities of gases through polymeric membranes. The developed model successfully applied to predict the permeabilities of gases through the pristine CA membrane for literature data as well for this work. The permeability prediction was made by certain deviations, which are associated with both membrane fabrication conditions as well as due to the use of different correlations. These correlations have their limitations, and the deviation can be overcome using other correlations that can take account of different conditions as well as the specific properties of the polymer and the permeating gas.

References

Aaron D, Tsouris C (2005) Separation of CO2 from flue gas: a review. Sep Sci Technol 40:321–348

Adam G, Gibbs JH (1965) On the temperature dependence of cooperative relaxation properties in glass-forming liquids. J Chem Phys 43:139–146

Baker RW, Low BT (2014) Gas separation membrane materials: a perspective. Macromolecules 47:6999–7013

Barrer RM (1942) Permeability in relation to viscosity and structure of rubber. Rubber Chem Technol 15:537–544

Car A, Stropnik C, Peinemann K-V (2006) Hybrid membrane materials with different metal–organic frameworks (MOFs) for gas separation. Desalination 200:424–426

Caro J, Noack M, Kölsch P, Schäfer R (2000) Zeolite membranes–state of their development and perspective. Microporous Mesoporous Mater 38:3–24

Chung T-S, Jiang LY, Li Y, Kulprathipanja S (2007) Mixed matrix membranes (MMMs) comprising organic polymers with dispersed inorganic fillers for gas separation. Prog Polym Sci 32:483–507

Cong H, Radosz M, Towler BF, Shen Y (2007) Polymer–inorganic nanocomposite membranes for gas separation. Sep Purif Technol 55:281–291

Dimarzio EA, Gibbs JH (1963) Molecular interpretation of glass temperature depression by plasticizers. J Polym Sci Part A 1:1417–1428

Dong G, Li H, Chen V (2013) Challenges and opportunities for mixed-matrix membranes for gas separation. J Mater Chem A 1:4610–4630

Esteves IA, Mota JP (2007) Gas separation by a novel hybrid membrane/pressure swing adsorption process. Ind Eng Chem Res 46:5723–5733

Farrukh S, Javed S, Hussain A, Mujahid M (2014a) Blending of TiO2 nanoparticles with cellulose acetate polymer: to study the effect on morphology and gas permeation of blended membranes. Asia Pac J Chem Eng 9:543–551

Farrukh S, Minhas FT, Hussain A, Memon S, Bhanger M, Mujahid M (2014b) Preparation, characterization, and applicability of novel calix [4] arene-based cellulose acetate membranes in gas permeation. J Appl Polym Sci 131

Flory P (1953) J, Am, Chem. Sac. 63 (1941) 3091 c) FLORY P. J., Principles of polymer chemistry. Comell University Press, Ithaca,

Ghosal K, Freeman BD (1994) Gas separation using polymer membranes: an overview. Polym Adv Technol 5:673–697

Gibbs JH, DiMarzio EA (1958) Nature of the glass transition and the glassy state. J Chem Physics 28:373–383

Haraya K, Obata K, Hakuta T, Yoshitome H (1986a) Permeation of gases through a symmetric cellulose acetate membrane. J Chem Eng Jpn 19:464–466

Haraya K, Obata K, Hakuta T, Yoshitome H (1986b) The permeation of gases through asymmetric cellulose acetate membranes. J Chem Eng Jpn 19:431–436

Hayashi H, Cote AP, Furukawa H, O'Keeffe M, Yaghi OM (2007) Zeolite A imidazolate frameworks. Nat Mater 6:501

Hillock AM, Miller SJ, Koros WJ (2008) Crosslinked mixed matrix membranes for the purification of natural gas: effects of sieve surface modification. J Membr Sci 314:193–199

Himma NF, Wardani AK, Prasetya N, Aryanti PT, Wenten IG (2018) Recent progress and challenges in membrane-based O2/N2 separation. Rev Chem Eng

Hu C-C, Liu T-C, Lee K-R, Ruaan R-C, Lai J-Y (2006) Zeolite-filled PMMA composite membranes: influence of coupling agent addition on gas separation properties. Desalination 193:14–24

Hu Y, Kazemian H, Rohani S, Huang Y, Song Y (2011) In situ high pressure study of ZIF-8 by FTIR spectroscopy Chem Commun 47: 12694–12696

Huang XC, Lin YY, Zhang JP, Chen XM (2006a) Ligand-directed strategy for zeolite-type metal–organic frameworks: zinc (II) imidazolates with unusual zeolitic topologies. Angew Chem Int Ed 45:1557–1559

Huang Z, Li Y, Wen R, May Teoh M, Kulprathipanja S (2006b) Enhanced gas separation properties by using nanostructured PES-zeolite 4A mixed matrix membranes. J Appl Polym Sci 101:3800–3805

Iqbal H, Farrukh S, Hussain A, Hassan A, Hailegiorgis SM (2019) Pursuance of Piper Nigrum and Cinnamomum verum on poly vinyl alcohol-starch hydrogel membrane. J Chem Soc Pak 41:489–500

Isfahani AP, Ghalei B, Bagheri R, Kinoshita Y, Kitagawa H, Sivaniah E, Sadeghi M (2016a) Polyurethane gas separation membranes with ethereal bonds in the hard segments. J Membr Sci 513:58–66

Isfahani AP, Ghalei B, Wakimoto K, Bagheri R, Sivaniah E, Sadeghi M (2016b) Plasticization resistant crosslinked polyurethane gas separation membranes. J Mater Chem A 4:17431–17439

Ismail AF, David L (2001) A review on the latest development of carbon membranes for gas separation. J Membr Sci 193:1–18

Kim JY, Bae YC (1999a) Configurational entropy effect for conductivities of solid polymer electrolytes. J Appl Polym Sci 73:1891–1897

Kim JY, Bae YC (1999b) Configurational entropy effect for the conductivity of semicrystalline polymer/salt systems. Fluid Phase Equilib 163:291–302

Kim GM, Michler G, Gahleitner M, Fiebig J (1996) Relationship between morphology and micromechanical toughening mechanisms in modified polypropylenes. J Appl Polym Sci 60:1391–1403

Kim JY, Hong SU, Won J, Kang YS (2000) Molecular model and analysis of glass transition temperatures for polymer− diluent− salt systems. Macromolecules 33:3161–3165

Kim S, Marand E, Ida J, Guliants VV (2006) Polysulfone and mesoporous molecular sieve MCM-48 mixed matrix membranes for gas separation. Chem Mater 18:1149–1155

Kim S, Chen L, Johnson JK, Marand E (2007) Polysulfone and functionalized carbon nanotube mixed matrix membranes for gas separation: theory and experiment. J Membr Sci 294:147–158

Koros WJ (2002) Gas separation membranes: needs for combined materials science and processing approaches. In: Macromolecular symposia. vol 1. Wiley Online Library, pp 13–22

Koros WJ, Fleming G (1993) Membrane-based gas separation. J Membr Sci 83:1–80

Koros WJ, Mahajan R (2000) Pushing the limits on possibilities for large scale gas separation: which strategies? J Membr Sci 175:181–196

Koros W, Fleming G, Jordan S, Kim T, Hoehn H (1988) Polymeric membrane materials for solution-diffusion based permeation separations. Prog Polym Sci 13:339–401

Lee DK, Kim YW, Lee KJ, Min BR, Kim JH (2007) Thermodynamic model of gas permeability in polymer membranes. J Polym Sci B Polym Phys 45:661–665

Li J, Wang S, Nagai K, Nakagawa T, Mau AW (1998) Effect of polyethyleneglycol (PEG) on gas permeabilities and permselectivities in its cellulose acetate (CA) blend membranes. J Membr Sci 138:143–152

Li Y, Chung T-S, Cao C, Kulprathipanja S (2005) The effects of polymer chain rigidification, zeolite pore size and pore blockage on polyethersulfone (PES)-zeolite A mixed matrix membranes. J Membr Sci 260:45–55

Li Y, Guan H-M, Chung T-S, Kulprathipanja S (2006) Effects of novel silane modification of zeolite surface on polymer chain rigidification and partial pore blockage in polyethersulfone (PES)–zeolite a mixed matrix membranes. J Membr Sci 275:17–28

Li Y, Chung TS, Kulprathipanja S (2007) Novel Ag+−zeolite/polymer mixed matrix membranes with a high CO2/CH4 selectivity. AICHE J 53:610–616

Ma S, Sun D, Simmons JM, Collier CD, Yuan D, Zhou H-C (2008) Metal-organic framework from an anthracene derivative containing nanoscopic cages exhibiting high methane uptake. J Am Chem Soc 130:1012–1016

MacFarlane D, Sun J, Meakin P, Fasoulopoulos P, Hey J, Forsyth M (1995) Structure-property relationships in plasticized solid polymer electrolytes. Electrochim Acta 40:2131–2136

Mahajan R, Burns R, Schaeffer M, Koros WJ (2002) Challenges in forming successful mixed matrix membranes with rigid polymeric materials. J Appl Polym Sci 86:881–890

Mark JE (2009) Polymer data handbook. Oxford university press, Oxford

Matteucci S, Yampolskii Y, Freeman BD, Pinnau I (2006) Transport of gases and vapors in glassy and rubbery polymers. Mater Sci Membr Gas Vap Sep 1:1–2

Merkel T, Bondar V, Nagai K, Freeman B, Pinnau I (2000) Gas sorption, diffusion, and permeation in poly (dimethylsiloxane). J Polym Sci B Polym Phys 38:415–434

Mersmann A, Fill B, Hartmann R, Maurer S (2000) The potential of energy saving by gas-phase adsorption processes. Chem Eng Technol 23:937–944

Minhas FT, Farrukh S, Hussain A, Mujahid M (2015) Comparison of silica and novel functionalized silica-based cellulose acetate hybrid membranes in gas permeation study. J Polym Res 22:63

Moore TT, Koros WJ (2007) Gas sorption in polymers, molecular sieves, and mixed matrix membranes. J Appl Polym Sci 104:4053–4059

Moore TT, Koros WJ (2008) Sorption in zeolites modified for use in organic− inorganic hybrid membranes. Ind Eng Chem Res 47: 591–598

Moore TT, Vo T, Mahajan R, Kulkarni S, Hasse D, Koros WJ (2003) Effect of humidified feeds on oxygen permeability of mixed matrix membranes. J Appl Polym Sci 90:1574–1580

Moore TT, Mahajan R, Vu DQ, Koros WJ (2004) Hybrid membrane materials comprising organic polymers with rigid dispersed phases. AICHE J 50:311–321

Mueller U, Schubert M, Teich F, Puetter H, Schierle-Arndt K, Pastre J (2006) Metal–organic frameworks—prospective industrial applications. J Mater Chem 16:626–636

Murali RS, Sankarshana T, Sridhar S (2013) Air separation by polymer-based membrane technology. Sep Purif Rev 42:130–186

Ordonez MJC, Balkus KJ Jr, Ferraris JP, Musselman IH (2010) Molecular sieving realized with ZIF-8/Matrimid® mixed-matrix membranes. J Membr Sci 361:28–37

Pandey P, Chauhan R (2001) Membranes for gas separation. Prog Polym Sci 26:853–893

Park KS et al (2006) Exceptional chemical and thermal stability of zeolitic imidazolate frameworks. Proc Natl Acad Sci 103:10186–10191

Patel R, Park JT, Hong HP, Kim JH, Min BR (2011) Use of block copolymer as compatibilizer in polyimide/zeolite composite membranes. Polym Adv Technol 22:768–772

Perez EV, Balkus KJ Jr, Ferraris JP, Musselman IH (2009) Mixed-matrix membranes containing MOF-5 for gas separations. J Membr Sci 328:165–173

Rehman A, Farrukh S, Hussain A, Pervaiz E (2019) Synthesis and effect of metal–organic frame works on CO2 adsorption capacity at various pressures: a contemplating review. Energy & Environment: 0958305X19865352

Reid BD, Ruiz-Trevino FA, Musselman IH, Balkus KJ, Ferraris JP (2001) Gas permeability properties of polysulfone membranes containing the mesoporous molecular sieve MCM-41. Chem Mater 13:2366–2373

Robeson LM (1991) Correlation of separation factor versus permeability for polymeric membranes. J Membr Sci 62:165–185

Rowe BW, Robeson LM, Freeman BD, Paul DR (2010) Influence of temperature on the upper bound: Theoretical considerations and comparison with experimental results. J Membr Sci 360:58–69

Sanders DF, Smith ZP, Guo R, Robeson LM, McGrath JE, Paul DR, Freeman BD (2013) Energy-efficient polymeric gas separation membranes for a sustainable future: a review. Polymer 54:4729–4761

Sen D, Kalipcilar H, Yilmaz L (2006) Development of zeolite filled polycarbonate mixed matrix gas separation membranes. Desalination 200:222–224

Sheffel JA, Tsapatsis M (2007) A model for the performance of microporous mixed matrix membranes with oriented selective flakes. J Membr Sci 295:50–70

Shu S, Husain S, Koros WJ (2007) A general strategy for adhesion enhancement in polymeric composites by formation of nanostructured particle surfaces. J Phys Chem C 111:652–657

Stern SA (1994) Polymers for gas separations: the next decade. J Membr Sci 94:1–65

Van Amerongen GJ (1946) The permeability of different rubbers to gases and its relation to diffusivity and solubility. J Appl Phys 17:972–985

Van Amerongen G (1964) Diffusion in elastomers. Rubber Chem Technol 37:1065–1152

van de Graaf JM, van der Bijl E, Stol A, Kapteijn F, Moulijn JA (1998) Effect of operating conditions and membrane quality on the separation performance of composite silicalite-1 membranes. Ind Eng Chem Res 37:4071–4083

Van Krevelen DW, Te Nijenhuis K (2009) Properties of polymers: their correlation with chemical structure; their numerical estimation and prediction from additive group contributions. Elsevier, Amsterdam

Vu DQ, Koros WJ, Miller SJ (2003a) Mixed matrix membranes using carbon molecular sieves: I. preparation and experimental results. J Membr Sci 211:311–334

Vu DQ, Koros WJ, Miller SJ (2003b) Mixed matrix membranes using carbon molecular sieves: II. modeling permeation behavior. J Membr Sci 211:335–348

Weitkamp J, Hunger M, Ceika J, van Bekkum H, Corma A, Schuth F (2007) Introduction to zeolite science and practice. Stud Surf Sci Catal 168:787–835

Yong HH, Park HC, Kang YS, Won J, Kim WN (2001) Zeolite-filled polyimide membrane containing 2, 4, 6-triaminopyrimidine. J Membr Sci 188:151–163

Zhang MQ, Rong MZ, Zhang HB, Friedrich K (2003) Mechanical properties of low nano-silica filled high density polyethylene composites. Polym Eng Sci 43:490–500

Zhang Y, Musselman IH, Ferraris JP, Balkus KJ Jr (2008a) Gas permeability properties of Matrimid® membranes containing the metal-organic framework Cu–BPY–HFS. J Membr Sci 313:170–181

Zhang Y, Musselman IH, Ferraris JP, Balkus KJ (2008b) Gas permeability properties of mixed-matrix matrimid membranes containing a carbon aerogel: a material with both micropores and mesopores. Ind Eng Chem Res 47:2794–2802

Zhou K, Mousavi B, Luo Z, Phatanasri S, Chaemchuen S, Verpoort F (2017) Characterization and properties of Zn/Co zeolitic imidazolate frameworks vs. ZIF-8 and ZIF-67. J Mater Chem A 5:952–957